

Structure and DNA binding activity of the mouse condensin hinge domain highlight common and diverse features of SMC proteins

Julia J. Griese, Gregor Witte and Karl-Peter Hopfner*

Department of Biochemistry, Gene Center, Center for Integrated Protein Sciences and Munich Center for Advanced Photonics, Ludwig-Maximilians University Munich, Feodor-Lynen-Str. 25, D-81377 Munich, Germany

Received December 22, 2009; Revised and Accepted January 14, 2010

ABSTRACT

Structural Maintenance of Chromosomes (SMC) proteins are vital for a wide range of processes including chromosome structure and dynamics, gene regulation and DNA repair. Eukaryotes have three SMC complexes, consisting of heterodimeric pairs of six different SMC proteins along with several specific regulatory subunits. In addition to their other functions, all three SMC complexes play distinct roles in DNA repair. Cohesin (SMC1–SMC3) is involved in DNA double-strand break repair, condensin (SMC2–SMC4) participates in single-strand break (SSB) repair, and the SMC5–SMC6 complex functions in various DNA repair pathways. SMC proteins consist of N- and C-terminal domains that fold back onto each other to create an ATPase ‘head’ domain, connected to a central ‘hinge’ domain via long coiled-coils. The hinge domain mediates dimerization of SMC proteins and binds DNA, but it is not clear to what purpose this activity serves. We studied the structure and function of the condensin hinge domain from mouse. While the SMC hinge domain structure is largely conserved from prokaryotes to eukaryotes, its function seems to have diversified throughout the course of evolution. The condensin hinge domain preferentially binds single-stranded DNA. We propose that this activity plays a role in the SSB repair function of the condensin complex.

INTRODUCTION

Throughout all kingdoms of life, Structural Maintenance of Chromosomes (SMC) proteins are responsible for the faithful inheritance of genetic information. They are involved in a wide range of vital cellular processes from

cell division to gene regulation and DNA repair, acting as global organizers and safeguards of the genome. Whereas prokaryotic genomes encode for only one SMC protein that exists as a homodimer, eukaryotes possess six different SMC proteins that form three distinct heterodimeric complexes, with the holocomplexes additionally containing several specific regulatory non-SMC subunits (1).

In prokaryotes, the SMC complex is required for chromosome condensation and segregation (2). In eukaryotes, the complex containing SMC1 and SMC3, named cohesin, is responsible for sister chromatid cohesion during mitosis and meiosis (3). The condensin complex with SMC2 and SMC4 at its core is required, but not solely responsible for proper chromosome condensation and segregation during cell division (4). It seems to organize and maintain the chromosome scaffold rather than actually establishing it (5,6), but how it accomplishes this function is still unresolved. The as yet unnamed SMC5–SMC6 complex is involved in several DNA repair pathways as well as homologous recombination in meiosis (7).

Both cohesin and condensin are also involved in gene regulation (8–13) and DNA repair (14–20). While their roles are partially overlapping, they seem to be involved in different DNA repair pathways. Cohesin on the one hand is specifically recruited to DNA double-strand breaks (DSBs) in postreplicative cells and promotes DNA repair from the sister chromatid (17,21,22). Induction of a single DSB indeed leads to genome-wide establishment of cohesion independently of DNA replication (23,24), thus cohesin acts like a safeguard of genome integrity.

The function of condensin in DNA repair on the other hand is less well-characterized. Studies in yeast have implied that condensin has an interphase-specific function in DNA repair, but they have not clarified which DNA repair pathway is affected (14,16). There are, however, indications that condensin is involved in DNA single-strand break (SSB) repair (25,26). There are two forms of condensin in vertebrates that differ in their

*To whom correspondence should be addressed. Tel: +49 89 2180 76953; Fax: +49 89 2180 76999; Email: hopfner@lmb.uni-muenchen.de

non-SMC subunits, but have the same core consisting of SMC2 and SMC4 (27). Human condensin I was shown to interact in an interphase-specific manner with the DNA nick-sensor poly(ADP-ribose) polymerase 1 (PARP1), and this interaction increased upon SSB damage induction. While nuclear retention of condensin was enhanced in the presence of SSBs, this was not the case for cohesin. Depletion of condensin I compromised SSB, but not DSB repair.

The interaction between condensin and PARP1 was particularly strong in S phase, suggesting an involvement of condensin also in normal DNA replication (25). Indeed, condensin was found to accumulate at stalled replication forks in budding yeast (28), and was shown to be required for the replication checkpoint response after stalling replication by hydroxyurea treatment in fission yeast (14). Since it is not known whether condensin is also found at moving replication forks, its presence at stalled forks might either be due to its DNA repair function, or a function in undisturbed DNA replication.

SMC proteins have a striking domain architecture consisting of a long antiparallel coiled-coil region with globular domains at both ends (1,29). Their N- and C-terminus interact at one end of the coiled-coil to make up an ATP-binding cassette (ABC)-type ATPase 'head' domain to which most of the non-SMC subunits bind. The 'hinge' domain at the other end of the coiled-coil mediates dimerization of SMC proteins. However, its function exceeds that of a simple dimerization domain, as it has previously been shown to bind DNA (30–33). In case of the *Bacillus subtilis* SMC protein, ATP binding to the head domains stimulates DNA binding to the hinge domains (33), and this in turn stimulates ATP hydrolysis by the head domains (31,32,34,35). This indicates that the hinge domain is capable of transmitting structural changes along the coiled-coil region to the head domains and vice versa.

Structures of two bacterial SMC hinge domains have been solved to date, namely that of the *Thermotoga maritima* SMC hinge (29) and that of the *Escherichia coli* MukB hinge (36,37). MukB is a divergent SMC protein, and its hinge domain is substantially smaller than that of the *T. maritima* SMC protein. Nonetheless the structures of the two hinge domains are quite similar. Two hinge domain monomers interact with each other via two interfaces to create a doughnut-shaped homodimer with 2-fold symmetry. The coiled-coils are formed intramolecularly and emerge from the same face of the dimer (29,36,37).

Most investigations focusing on the hinge domain have so far been conducted with bacterial SMC proteins. To shed more light on the structure and function of eukaryotic SMC hinges, we focused our efforts on the condensin hinge domain from mouse. We solved its atomic resolution crystal structure and furthermore studied its DNA binding activity. Interestingly, the condensin hinge domain preferentially binds single-stranded DNA (ssDNA), while its interaction with double-stranded DNA (dsDNA) is non-specific. Taking into account the data placing condensin in SSB repair

(25), we propose that the ssDNA binding activity of the hinge domain supports the DNA repair function of the condensin complex.

MATERIALS AND METHODS

Cloning, expression and protein purification

We designed two mouse condensin hinge domain constructs of different lengths. The longer construct, designated mSMC2h4h-l, spans residues 492–680 of SMC2, and residues 581–766 of SMC4, while the shorter one, mSMC2h4h-s, contains residues 506–666 of SMC2, and residues 595–752 of SMC4. DNA fragments encoding the desired hinge domain constructs were PCR-amplified from cDNA vectors (SMC2: image ID 30543190; SMC4: image ID 6841276, imaGenes) and cloned into a modified bicistronic pET-21b vector (Novagen) carrying a second ribosome binding site between the SalI and NotI sites. The *smc2* hinge fragment was inserted between the NdeI/EcoRI sites, and the *smc4* hinge fragment was cloned into the NcoI/XhoI sites to be expressed with the vector-encoded C-terminal hexahistidine tag. In the long construct, the SMC2 subunit additionally carries an N-terminal Strep II tag (38) added via the PCR primer. Point mutations were introduced into the vectors by site-directed mutagenesis using the QuikChange method (Stratagene). All constructs were verified by sequencing.

Expression was carried out in *E. coli* Rosetta (DE3) (Novagen). Cultures were grown at 37°C in LB medium supplemented with the appropriate antibiotics to an optical density (600 nm) of ~0.7, cooled down to 18°C, and induced with 0.5 mM IPTG. Cells were harvested by centrifugation 20 h after induction. Cell pellets were stored at –20°C until further use. To obtain selenomethionine-labelled protein, constructs were expressed in *E. coli* B834 (DE3) additionally containing the pRARE plasmid (Novagen) in LeMaster's medium (39) supplemented with the appropriate antibiotics and selenomethionine.

Proteins were purified via nickel chelate affinity chromatography and gel filtration. All purification steps were carried out at 8°C. Cells from 2 l of culture were lysed by sonication in buffer A (25 mM Tris-HCl pH 8.0, 300 mM NaCl, 20 mM imidazole). The lysate was cleared by centrifugation and applied to a gravity flow column containing Ni-NTA agarose beads (Qiagen). Nickel chelate chromatography was performed using buffer A for washing and buffer B (25 mM Tris-HCl pH 8.0, 300 mM NaCl, 250 mM imidazole) for elution. The eluate was concentrated in centrifugal filter units (Amicon Ultra, 10 000 MWCO, Millipore) and applied to a Superdex 200 pg 26/60 gel filtration column (GE Healthcare) equilibrated in buffer C (5 mM Tris-HCl pH 8.0, 100 mM NaCl, 0.1 mM EDTA). Fractions containing only the heterodimeric SMC2–SMC4 hinge domain were pooled, and the protein was concentrated to 30–40 mg/ml. Protein concentration was determined using a calculated extinction coefficient at 280 nm (40). The purification process was monitored by SDS-PAGE (41). Concentrated protein was aliquoted, flash frozen in

liquid nitrogen and stored at -80°C until further use. Selenomethionine-labelled protein was purified analogously with the addition of 1 mM DTT to all buffers. TCEP was added to the concentrated protein to a final concentration of 1 mM to prevent oxidation of the selenomethionine residues.

Small-angle X-ray scattering of protein solutions

To prepare samples suitable for small-angle X-ray scattering (SAXS) measurements, proteins were additionally purified via gel filtration on a Superdex 200 column (GE Healthcare), and concentrated to yield samples in concentration ranges from 2 to 20 mg/ml in buffer C. The flowthrough of the concentration step was used as buffer reference for SAXS measurements. SAXS data were collected at beamline X33 at EMBL/DESY, Hamburg. Scattering profiles of BSA and lysozyme were measured as reference for molecular mass determination. The ATSAS package (42) was used to process and analyze data. Theoretical scattering profiles from atomic resolution models were calculated and fitted to measured profiles with CRY SOL. *Ab initio* models of mSMC2h4h-l were reconstructed from the experimental data using the program GASBORp without imposing any symmetry or other restrictions on possible models. Ten independently reconstructed envelopes were aligned and averaged with SUPCOMB and DAMAVER. Envelope representations were calculated using the Situs package (43), which was also used to dock atomic resolution models into the envelope.

Protein crystallization and structure determination

The short mouse condensin hinge construct mSMC2h4h-s was crystallized by vapor diffusion in the hanging-drop setup at 20°C . Crystallization was optimized with selenomethionine-labelled protein. The refined crystallization condition contained 15% (w/v) PEG 4000, 5% (v/v) isopropanol, 20% (v/v) glycerol and 100 mM Tris-HCl pH 8.5. For data collection, crystals were flash-frozen in liquid nitrogen without additional cryoprotection. Data were collected at beamline PXI of the Swiss Light Source (SLS, Villigen, Switzerland). The crystals belong to space group $P2_1$ and contain one molecule each of the SMC2 and SMC4 subunits in the asymmetric unit (see Supplementary Table S1 for crystallographic data, phasing and refinement statistics). The structure was determined by single-wavelength anomalous dispersion (SAD) phasing from a peak wavelength dataset of the selenomethionine-labelled protein crystals. Data were indexed and integrated using the XDS package (44). Phases were calculated with AutoSHARP (45). The model was largely automatically built with ARP/wARP (46–48) and completed by manual model building in Coot (49). Initial refinement was carried out with CNS (50), followed by several rounds of refinement with phenix.refine (51) and rebuilding in Coot. Refinement included simulated annealing in initial cycles, individual atomic coordinate and anisotropic B factor refinement, and bulk solvent corrections. Solvent molecules were

added with phenix.refine and manually. The R_{free} factor was calculated from 10% of the data which were removed at random before the structure was refined. The structure was validated using MolProbity (52) and PROCHECK (53). The electrostatic surface potential was calculated with the Adaptive Poisson–Boltzmann Solver (APBS) (54). All figures were prepared with PyMOL (DeLano, W.L. The PyMOL Molecular Graphics System. (2008) DeLano Scientific LLC, Palo Alto, CA, USA. <http://www.pymol.org>). Coordinates and structure factors were deposited at the Protein Data Bank (PDB) with accession number 3L51.







In vitro DNA-binding assays

We used DNA oligonucleotide substrates carrying a 6-FAM fluorescence label to monitor their binding to the mouse condensin hinge domain (Table 1). HPLC-purified DNA oligonucleotides (Thermo Scientific) were dissolved in water. DNA concentration was determined using a calculated extinction coefficient at 260 nm (55). To anneal oligonucleotides, they were mixed with a 1.1-fold molar excess of the unlabelled oligonucleotide in 40 mM Tris-HCl pH 7.5, 100 mM NaCl, 10 mM MgCl_2 , incubated in a thermocycler (Biometra T personal) for 5 min at 95°C , and then cooled down to 4°C at a cooling rate of 0.1°C/s .

Samples for electrophoretic mobility shift assays (EMSA) contained 12.5 nM of a DNA substrate and protein in a 0-, 1-, 2-, 10-, 25-, 50-, 100-, 250-, 500- and 1000-fold molar excess over the DNA in $1 \times$ PBS in a total volume of 20 μl . They were incubated at room temperature for 30 min before addition of 5 μl 50% (v/v) glycerol. The samples were then loaded onto a 0.5% (w/v) agarose gel in $1 \times$ TB buffer and separated for 2 h at 4 V/cm and 8°C . Gels were scanned on a Typhoon 9400 fluorescence scanner (GE Healthcare).

Fluorescence quenching titrations were performed in a Horiba Jobin Yvon FluoroMax-P fluorimeter, using a 1.5 ml fluorescence cuvette with a stirring bar, at 20°C under constant stirring. The titration solution contained 25 nM 6-FAM-labelled DNA substrate (Table 1) in $1 \times$ PBS in a starting volume of 800 μl . Protein was added successively from a concentrated stock solution. After each addition of protein, the mixture was allowed to reach equilibrium for 1 min before measuring fluorescence. 6-FAM fluorescence was excited at 495 nm, and measured at the experimentally determined emission maximum of the DNA substrate (between 415 and 418 nm). Excitation and emission slit width were adjusted so that the signal was in the linear range of the photon counting multiplier. All measurements were performed in triplicate. Data were normalized and fitted using a non-linear least squares fit algorithm with a single-site binding model. Dissociation constants are the result of global fits to triplicates, errors are the standard deviations of dissociation constants resulting from independent fits to the three measurements.

Table 1. Oligonucleotides used for DNA-binding assays

Name	Structure	Oligonucleotide sequences
30-mer ssDNA		5'-6-FAM-TTTTTTTTTTTTTTTTTTTTTTTTTTTTTTTTTTTT
15-mer ssDNA		5'-6-FAM-TTTTTTTTTTTTTTTT
30-mer dsDNA		strand 1: 5'-6-FAM-CCGGAAGCATCTAGCATCCTGTCCAGCTGC strand 2: 5'-GCAGCTGACAGGATGCTAGATGCTTTCCGG
30-mer ds-ssDNA-3'		strand 1: 5'-6-FAM-CATCCTGTCCGCTGC strand 2: 5'-GCAGCGGACAGGATGTTTTTTTTTTTTTTTTTTT
30-mer ds-ssDNA-5'		strand 1: 5'-6-FAM-CATCCTGTCCGCTGC strand 2: 5'-TTTTTTTTTTTTTTTTCAGCGGACAGGATG
45-mer ds-ss-dsDNA		strand 1: 5'-6-FAM-CATCCTGTCCGCTGC strand 2: 5'-CCGAGAGCATCTCG strand 3: 5'-GCAGCGGACAGGATGTTTTTTTTTTTTTTTTTTCAGATGCTCTCCGG

The 5'-end is on the left side for the single-stranded substrates and the top strand(s) of double-stranded substrates. The diamond symbolizes the 6-FAM fluorescence label.

RESULTS

Protein purification, crystallization and structure determination

To facilitate crystallization, we designed two expression constructs of the mouse SMC2-SMC4 hinge domain. The longer construct, designated mSMC2h4h-l (residues 492-680 of SMC2 and 581-766 of SMC4), was designed to contain a short stretch of coiled-coil at both ends, while the shorter one, mSMC2h4h-s (residues 506-666 of SMC2 and 595-752 of SMC4), does not contain any coiled-coil segments. Both constructs were expressed in *E. coli*, and the proteins were purified via nickel chelate affinity chromatography and gel filtration to yield stable heterodimeric SMC2-SMC4 hinge domains. We obtained well diffracting crystals of mSMC2h4h-s in space group P2₁ with one heterodimer in the asymmetric unit. Selenomethionine derivative crystals diffracted to 1.5 Å resolution and allowed us to determine the phases by SAD. The resulting electron density map was of very high quality so that ~90% of the model could be built automatically. After several cycles of manual model building and refinement, the final *R* factors were 14.3% for *R*_{work} and 17.3% for *R*_{free}. The final model spans residues 506-660 of SMC2 and residues 595-752 of SMC4 including the entire hexahistidine tag, and has very good geometry. Crystallographic data, phasing and refinement statistics are shown in Supplementary Table S1, an example of the initial and refined electron density can be found in Supplementary Figure S1.

Crystal structure of the mouse condensin hinge domain

The SMC2 and SMC4 hinge subunits assemble into a heterodimer. Each subunit forms a half-ring structure with an α -helical core that is bordered by a mixed β -sheet on both sides (Figure 1A). The β -sheets are again flanked on the outside by one or two α -helices. Like the *T. maritima* SMC (TmaSMC) hinge domain (29), both subunits consist of two subdomains linked by a long but ordered loop that passes along the bottom face of the hinge, i.e. the face on the opposite side of the coiled-coils (Figure 1A). This loop lies between β -strand 3 and α -helix F of the SMC2 hinge, and between helices F and G of the SMC4 hinge (see the sequence alignment in

Figure 2 and the topology diagram in Supplementary Figure S2).

The TmaSMC (29) and the *E. coli* MukB (36,37) hinge domains form 2-fold-symmetric doughnut-shaped homodimers via two dimerization interfaces. Unexpectedly, the SMC2 and SMC4 hinge dimerize via only one interface and thus do not adopt the expected doughnut-shape (Figure 1A and B). The subunit interface is made up largely by two interacting β -strands, namely mSMC2h β 3 and mSMC4h β 7, to form a continuous mixed seven-stranded β -sheet (mSMC2h β 1-3 + mSMC4h β 4-7). Additional dimer interactions are contributed by helices α E of mSMC2h and α I of mSMC4h which flank the β -sheet on the outside (Figures 1A, B and 2, Supplementary Figure S2).

At the opposite side of the half-rings, the SMC2 hinge has a four-stranded and the SMC4 hinge a three-stranded mixed β -sheet (mSMC2h β 4-7, mSMC4h β 1-3), but these do not interact in our crystal form (Figure 1A and B). In fact, the angle between the two subunits is much wider than in the TmaSMC hinge homodimer (29), the hinge being thus bent along the intact interface to open up the ring at the opposite side. Superposition with the TmaSMC hinge structure reveals the probable reason for this partially open conformation: it seems that the SMC2 hinge is missing the last C-terminal β -strand that would be the one to interact with the outermost β -strand of the SMC4 hinge (β 3) to form a pseudo-2-fold symmetric dimer. The residues that are predicted to make up this β -strand are part of the crystallized construct, but are evidently disordered. SAXS analysis (see below) suggests that the SMC2-SMC4 hinge can also adopt a closed, doughnut-shaped structure which is presumably stabilized by the coiled-coil domains missing in our crystallized construct. There are no apparent crystal contacts that could have forced the hinge domain into this open conformation. We modelled the expected 'closed' conformation by separately superposing the SMC2 and SMC4 subunit of the mouse condensin hinge structure with the TmaSMC hinge domain dimer (Figure 1B). While this model produces some clashes at the intact interface and therefore obviously does not perfectly represent the biologically relevant closed conformation, it does show quite clearly that the C-terminal β -strand of the SMC2 hinge is indeed

missing to close the ring. The structural similarity to the TmaSMC hinge domain however strongly suggests that the subunit cores are correctly folded. The rmsd between the C α traces of the SMC2 and SMC4 hinge domain and the TmaSMC hinge (pdb 1GXL) is 2.2 and 2.6 Å, respectively, and the rmsd between the SMC2 and the SMC4 hinge is only 1.8 Å. Most secondary-structure elements are conserved.

Notable differences in secondary structure between the TmaSMC and the mouse condensin hinge domain are found in the SMC4 subunit (Figures 1C and 2, Supplementary Figure S2). In the mSMC2 and TmaSMC hinge domain, the N-terminal β -sheet merges directly into the long loop connecting the subdomains which terminates in a helix on the outside of the C-terminal β -sheet (mSMC2h α F). This helix is followed by a strand of the C-terminal β -sheet (mSMC2h β 4). The mSMC2 and mSMC4 hinges have the same number of helices, but their F helices do not correspond to each other and are in completely different positions, flanking the C-terminal β -sheet in mSMC2h, and the helical core on the outside surface in mSMC4h. In the mSMC4 hinge, helix F lies between the N-terminal β -sheet and the connecting loop which terminates in helix G of the helical core, so that the C-terminal β -sheet of mSMC4h consists of one less strand than that of the mSMC2 and TmaSMC hinge (provided that the predicted C-terminal β -strand of mSMC2h is indeed formed).

The SMC2–SMC4 hinge interface explains dimerization specificity of eukaryotic SMC proteins

Most intersubunit contacts are formed by hydrophobic interactions, supported by few hydrogen bonds (Figure 3). It has long been unclear how eukaryotic SMC proteins specifically assemble into defined

heterodimers (e.g. SMC1–SMC3, SMC2–SMC4), while prokaryotic SMC proteins form homodimers. Taking a closer look at the interface, the reason for dimerization specificity is revealed. While most residues contributing to the interaction are conserved or replaced by similar residues within the subfamilies SMC2/SMC3 and SMC1 α /SMC4 (56), the few non-conservative exchanges are apparently enough to make wrong pairing impossible. For SMC2/SMC3, good candidate residues for dimerization specificity within the N-terminal interface are K⁵⁷⁰R⁵⁷¹R⁵⁷² of SMC2 which are replaced by P⁵⁸²G⁵⁸³E⁵⁸⁴ in SMC3 (Figure 2). These residues are placed in an otherwise conserved region, hence it is very likely that they are in similar positions in the SMC2 and SMC3 tertiary structures. Looking at the dimerization interface, it is immediately obvious that the PGE sequence in SMC3 would not be able to form the same interactions with SMC4 as the KRR sequence in SMC2 (Figure 3). For example, SMC2-R⁵⁷² forms a hydrogen bond with the backbone oxygen of SMC4-G⁷⁴⁰. The shorter glutamate side chain in SMC3 could not support this interaction. Between the SMC4 and SMC1 α C-terminal interface residues there is only one non-conservative exchange, namely SMC4-T⁷²³ for SMC1 α -R⁶²⁶ (Figure 2). Again, this residue is situated in an otherwise conserved region. Assuming that it therefore adopts a similar position in SMC1 α as in SMC4, the arginine side chain would clash with K⁵⁶¹ of SMC2, thus making it impossible for SMC1 α to dimerize with SMC2. SMC3 on the other hand has a small threonine residue in place of SMC2-K⁵⁶¹, so that the SMC3 interface can accommodate the large side chain of SMC1 α -R⁶²⁶.

Solution scattering analysis shows that the condensin hinge domain can also adopt a closed conformation

To acquire structural information about the conformation of the condensin hinge in solution, we measured SAXS profiles of both the short and the long hinge domain construct (Figure 4A). The best data were obtained with protein concentrations of 8 and 20 mg/ml for the short and long construct, respectively. While the short construct showed a slight tendency to aggregate at high concentrations, the long construct did not show any such signs even at 20 mg/ml, thus yielding data of very high quality with little noise even at higher values of the scattering vector. The molecular mass determined from the scattering intensity extrapolated to zero angle confirms that both constructs exist as heterodimers in solution. We compared the observed scattering profiles with SAXS profiles calculated from the crystal structure and the model of the closed conformation (Figure 4A). The observed profile of mSMC2h4h-s matches perfectly with the profile calculated from the crystal structure. This means that the crystallized construct mSMC2h4h-s adopts the same open conformation in solution as in the crystal. Hence, this conformation is not produced by crystal contacts.

The long construct mSMC2h4h-l, on the other hand, clearly exhibits a different conformational state. The SAXS profiles suggest that this construct has the

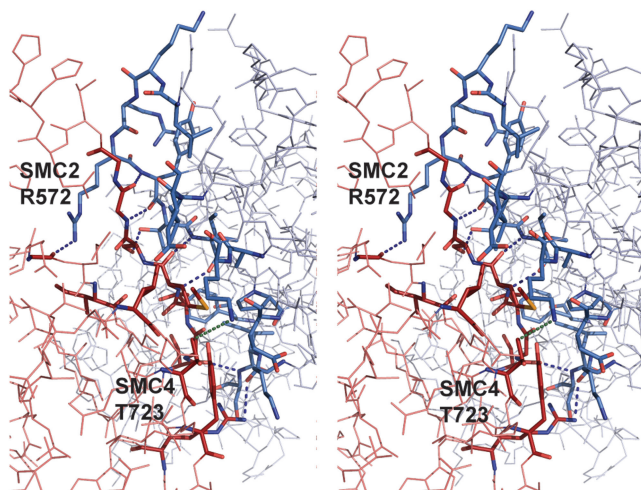


Figure 3. Stereo view of the interface between the SMC2 and SMC4 hinge. Residues contributing to the subunit interaction are shown as stick models with carbon atoms color blue and dark red for the SMC2 and SMC4 subunit, respectively, nitrogen: dark blue, oxygen: light red, and selenium: orange. The surrounding residues are depicted as thin lines in light blue for SMC2, and rose for SMC4. Hydrogen bonds are represented by dashed blue lines. The 5.5 Å distance between SMC2-K⁵⁶¹ and SMC4-T⁷²³ is indicated by a dashed green line.

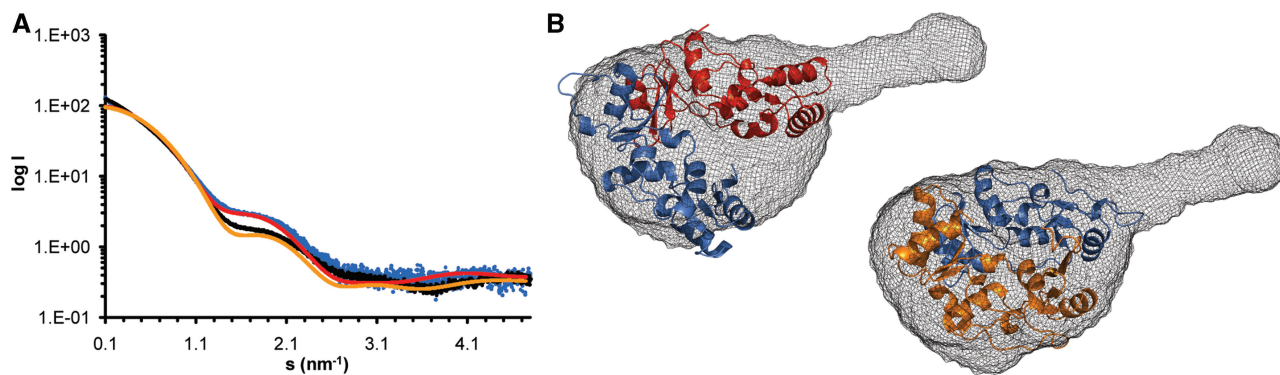


Figure 4. Small-angle X-ray scattering analysis of the mouse condensin hinge domain. (A) SAXS profiles of the short and long construct in solution in comparison with profiles calculated from atomic resolution models. The scattering profile of the long construct mSMC2h4h-l is shown in black, the profile of the short construct mSMC2h4h-s in blue. The calculated scattering profiles of the atomic resolution models of mSMC2h4h-s in the open and closed conformation are shown in red and orange, respectively. (B) Solution envelope reconstruction of the long construct mSMC2h4h-l, superimposed with the atomic resolution models of mSMC2h4h-s in the open (top left) and closed conformation (bottom right). The SAXS envelope is shown as grey mesh, the atomic resolution models are depicted in cartoon representation with the SMC2 subunit colored blue, and the SMC4 subunit colored red in the open and orange in the closed conformation.

expected closed conformation, as its scattering profile more closely resembles that of the closed than that of the open conformation (Figure 4A). We calculated 10 independent *ab initio* envelope reconstructions of the long construct. Due to the high data quality, there is a hint of the hole in the hinge heterodimer ring even in the averaged low-resolution envelope (Figure 4B). The stalk that sticks out on one side of the globular protein is big enough to contain 20–25 residues of an ordered loop or coiled-coil (Supplementary Figure S3). The construct mSMC2h4h-l is 14 residues longer than mSMC2h4h-s at all ends, and the SMC2 subunit additionally carries an N-terminal Strep II tag (eight residues). It is therefore most likely that the stalk consists of a short stretch of coiled-coil plus the Strep II tag of the SMC2 subunit (see Supplementary Figure S3 for an exemplary superposition of a crystal structure of a Strep II tag onto the stalk), while the ends of the SMC4 subunit are flexible in solution. Superposition of the open and closed conformation of mSMC2h4h-s onto the SAXS envelope shows a clearly better fit for the closed conformation. The open conformation does not completely fill the envelope whilst still projecting outside it, whereas the closed conformation nicely fills the globular part of the envelope. DNA binding data also imply that the long construct has two intact dimer interfaces (see below). Thus, we conclude that the long construct mSMC2h4h-l adopts the expected closed conformation.

The condensin hinge domain preferentially binds ssDNA

Previous work has demonstrated that the SMC hinge domain can bind DNA (30–33), but because of the purely qualitative nature of the assays performed in these studies, the specificity for different DNA substrates could not be unambiguously determined. To learn more about the potential role of the condensin complex in SSB repair, we quantitatively analyzed different DNA substrates for binding to the mouse condensin hinge domain. Sequences and structures of the DNA substrates

used can be found in Table 1. The short construct mSMC2h4h-s binds DNA only very weakly and non-specifically (Supplementary Figure S4 and data not shown), probably due to its partially open conformation or the lack of the transition into the coiled-coil region which might harbor additional DNA binding sites. The long construct mSMC2h4h-l, however, which adopts a closed conformation and contains a short stretch of the coiled-coil regions, binds DNA quite efficiently and shows interesting differential affinity towards different DNA substrates.

We performed EMSAs with 6-FAM-labelled DNA substrates (Supplementary Figure S4). The results suggest a qualitatively different binding behavior towards ssDNA and dsDNA. ssDNA was shifted upwards of the well, that is, the protein–ssDNA complex migrated towards the cathode, suggesting that the protein is so positively charged that even the complex with a 30-mer ssDNA oligonucleotide still has a surplus of positive charge. In fact, the long mouse condensin hinge construct has a theoretical isoelectric point of ~ 9.3 , and positively charged residues are distributed all over the surface of the protein (Figure 6). While a 30-mer dsDNA substrate was also bound, the EMSAs implied that it was bound much more weakly than the ssDNA substrate of the same length (Supplementary Figure S4). Also, the protein–dsDNA complex did not migrate towards the cathode, but remained in the wells. Thus, EMSAs are not the method of choice to quantitatively analyze DNA binding.

We therefore performed fluorescence quenching titrations to get a better picture of the DNA binding activity of the mouse condensin hinge, exploiting the fact that binding of 6-FAM-labelled DNA to the mouse condensin hinge leads to quenching of 6-FAM fluorescence. The resulting titration curves are not only a means to quantify the affinity towards different DNA substrates with great accuracy, but also contain information about the binding mode. All measurements were performed at physiological salt concentrations. Inclusion of Mg^{2+} in

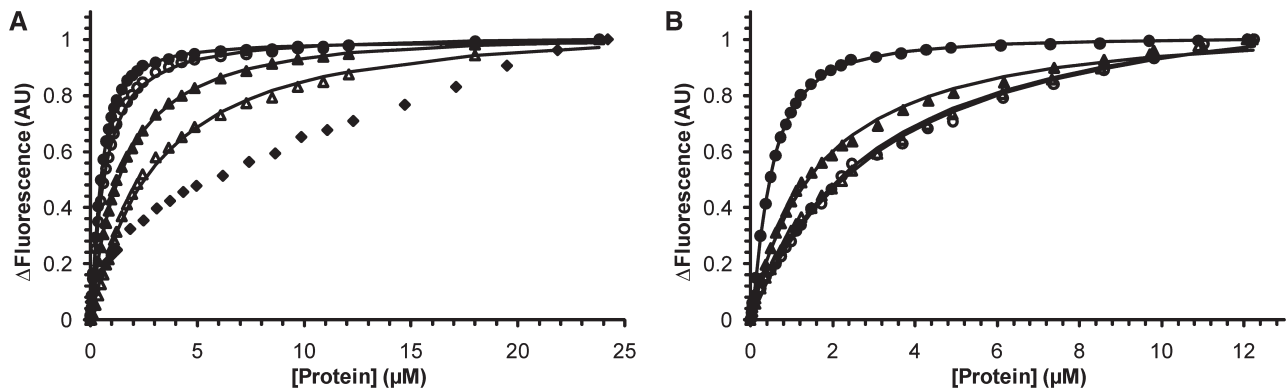


Figure 5. Fluorescence quenching titrations. One representative titration curve of each triplicate measurement is shown. Solid lines represent fits according to a single-site binding model. (A) Titrations of different DNA substrates with the long mouse condensin hinge domain construct mSMC2h4h-1 wt. DNA substrates are: filled circles, 30-mer ssDNA; open circles, 45-mer ds-ss-dsDNA; filled triangles, 30-mer ds-ssDNA-3'; open triangles, 15-mer ssDNA; filled diamonds, 30-mer dsDNA. The titration with the 30-mer dsDNA substrate could not be fitted with a simple binding model. For clarity, the titration with the 30-mer ds-ssDNA-5' substrate is not shown. For structures and sequences of the DNA substrates see Table 1. (B) Titrations of the 30-mer ssDNA substrate with mSMC2h4h-1 and three point mutants. Proteins are: filled circles, mSMC2h4h-1 wt; filled triangles, mSMC2h^{K566E}4h-1; open circles, mSMC2h^{K566E}4h^{K657E}-1; open triangles, mSMC2h^{K613E}4h^{K698E}-1. All titrations were performed with 25 nM of the 6-FAM labelled DNA substrate in 1 \times PBS at 20°C in a Horiba Jobin Yvon FluoroMax-P fluorimeter.

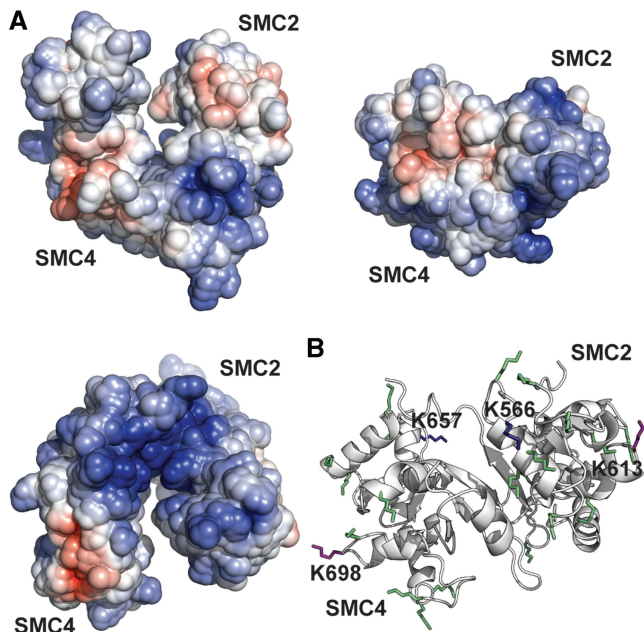


Figure 6. (A) Electrostatic surface potential of the mouse condensin hinge domain. Positively charged regions are colored blue, negatively charged regions red, and neutral regions white. The panels, from top left to bottom, show the top face, the view from the side onto the closed interface, and the bottom face. (B) Lysine residues in the mouse condensin hinge domain. The backbone of the condensin hinge is shown in cartoon representation in white, lysines are shown as stick models in green. Lysine residues mutated to glutamate in the point mutants SMC2-K^{566E}/SMC4-K^{657E} and SMC2-K^{613E}/SMC4-K^{698E} of mSMC2h4h-1 are colored blue and purple, respectively.

the assay buffer did not have any influence on DNA binding by the condensin hinge (data not shown). As can be seen in Figure 5A, the binding to dsDNA does not reach saturation even at a 1000-fold excess of protein and cannot be fitted using a simple binding model. This non-saturation behavior shows that the mouse condensin hinge binds dsDNA non-specifically.

We therefore conclude that non-specific binding produces such large protein-DNA aggregates that they cannot enter the gel matrix and remain in the wells in EMSAs.

On the other hand, the mouse condensin hinge domain binds all DNA substrates tested that are at least partially single-stranded specifically and with high affinity (Figure 5A and Table 2). We used oligo(dT) as ssDNA substrate because it does not form intramolecular base pairing or stacking interactions and is a model substrate to study ssDNA binding specificity (57). All titration curves obtained with partially or completely single-stranded substrates could be fitted using a single-site binding model, meaning that one hinge heterodimer binds one DNA molecule. The 30-mer ssDNA substrate is bound with a dissociation constant of $0.45 \pm 0.04 \mu$ M. A 15-mer ssDNA substrate is still bound specifically, albeit with an ~ 10 -fold higher dissociation constant ($K_d = 3.21 \pm 0.14 \mu$ M), suggesting that ~ 15 nucleotides constitute the minimal binding length. We presumed that the condensin hinge might fall off the ends of this short oligonucleotide, while it would not so quickly dissociate from the twice as long 30-mer ssDNA substrate. To test this hypothesis, we designed 15-mer ssDNA substrates that are 'capped' on one or both ends by a 15-mer dsDNA stretch. Indeed, the 30-mer ds-ssDNA substrate, where one end is capped, is bound twice as strongly as the 15-mer ssDNA. Dissociation constants were found to be the same within the range of error, regardless of whether the ssDNA stretch was a 3' or 5' overhang ($K_d = 1.55 \pm 0.05 \mu$ M for 30-mer ds-ssDNA-3', $1.77 \pm 0.08 \mu$ M for 30-mer ds-ssDNA-5'). This rules out specific recognition of a particular ssDNA-dsDNA transition by the condensin hinge. Since the fluorescence label is on the 5'-end of the short 15-mer strand (Table 1), it is close to the ssDNA stretch in the 30-mer ds-ssDNA-3' substrate and far away from it in the 30-mer ds-ssDNA-5' substrate. Titrations with these two substrates also showed that only the ssDNA stretch is bound, as the

absolute change in fluorescence intensity during the titration was half as big when the label was far away from the ssDNA stretch as when it was close to it. Capping both ends of the 15-mer ssDNA results in a 5-fold tighter binding with respect to the uncapped 15-mer ssDNA ($K_d = 0.66 \pm 0.02 \mu\text{M}$), hence the condensin hinge binds the 45-mer ds–ss–dsDNA substrate almost as tightly as the 30-mer ssDNA substrate. This suggests that the hinge domain is held in place on the ssDNA stretch by the dsDNA caps, making it less likely to dissociate. Although at least two protein molecules should theoretically fit onto the 45-mer ds–ss–dsDNA substrate, data could be fitted very well with a single-site binding model, giving further proof that in partially double-stranded and partially single-stranded substrates only the ssDNA stretch is bound by the condensin hinge.

Having shown that the mouse condensin hinge preferentially binds ssDNA, we wanted to characterize this binding more closely. We therefore made three lysine-to-glutamate point mutants of the long construct mSMC2h4h-l using site-directed mutagenesis: a single mutant mSMC2h^{K566E}4h-l, and two double mutants, mSMC2h^{K566E}4h^{K657E}-l, and mSMC2h^{K613E}4h^{K698E}-l. The first combination of lysine residues (SMC2-K⁵⁶⁶/SMC4-K⁶⁵⁷) was chosen because this is the only lysine residue that is highly conserved among SMC proteins from all species (Figure 2). The second combination was chosen due to the position of these lysine residues in the structure. While SMC2-K⁵⁶⁶/SMC4-K⁶⁵⁷ are at the C-terminus of α -helix E, the helix capping off the dimer interface, SMC2-K⁶¹³/SMC4-K⁶⁹⁸ are $\sim 90^\circ$ removed from the dimer interface, in the short loop connecting helices G and H, on the outside surface of the hinge domain (Figures 2 and 6B). Additionally, they are positioned in a region of the protein where the electrostatic surface potential is almost neutral, whereas there is a cluster of positively charged residues around the dimer interface (Figure 6A). All point mutant constructs behaved like the wild-type construct mSMC2h4h-l during purification. To confirm that the mutations do not disturb the protein fold, we measured SAXS profiles of all three mutant proteins which matched the profile of wild-type mSMC2h4h-l, although the mutant proteins, especially mSMC2h^{K613E}4h^{K698E}-l, displayed a higher tendency to aggregate than the wild-type protein (Supplementary Figure S5).

EMSA showed a reduction of the non-specific dsDNA binding for the single mutant and even more dramatically for both double mutants (Supplementary Figure S4), but results with the 30-mer ssDNA substrate were less clear. This is likely to be due to the fact that EMSAs are unsuitable to reveal subtle differences in binding strength (10-fold and less), as our data show. Fluorescence quenching titrations of the 30-mer ssDNA substrate with the mutant proteins clearly demonstrate a reduction in affinity as compared to wild-type (Figure 5B and Table 2). The effect of the mutations is additive, since the dissociation constant for the single mutant mSMC2h^{K566E}4h-l is half as big as that of the corresponding double mutant. Both double mutants have roughly the same affinity towards the 30-mer ssDNA, it is reduced

Table 2. Dissociation constants of complexes of the mouse condensin hinge with different DNA substrates

Protein construct	DNA substrate	K_d (μM)
mSMC2h4h-l wt	30-mer ssDNA	0.45 ± 0.04
	15-mer ssDNA	3.21 ± 0.14
	30-mer dsDNA	n.d.
	30-mer ds–ssDNA-3'	1.55 ± 0.05
	30-mer ds–ssDNA-5'	1.77 ± 0.08
	45-mer ds–ss–dsDNA	0.66 ± 0.02
mSMC2h ^{K566E} 4h-l	30-mer ssDNA	1.80 ± 0.08
mSMC2h ^{K566E} 4h ^{K657E} -l	30-mer ssDNA	3.26 ± 0.58
mSMC2h ^{K613E} 4h ^{K698E} -l	30-mer ssDNA	2.95 ± 0.30

The titration curves from the fluorescence quenching titrations were fitted using a single-site binding model. Dissociation constants K_d are the result of global fits to triplicate measurements, errors are the standard deviations of dissociation constants resulting from independent fits to the three measurements. For structures and sequences of the DNA substrates see Table 1. n.d., not determined.

7- to 8-fold as compared to wild-type. The mutations also reduce specificity of binding, as the titrations show a contribution of non-specific interaction. Especially for the double mutants, the binding does not saturate completely, and data could only be fitted up to a 500-fold excess of protein over DNA.

DISCUSSION

To learn more about the mechanism of eukaryotic SMC proteins, we determined the structure of a eukaryotic, heterodimeric SMC hinge domain from the mouse condensin complex, and quantitatively analyzed its DNA binding activity and specificity.

Our structure shows that the SMC hinge domain fold is conserved from prokaryotes to eukaryotes. Although the SMC2–SMC4 hinge heterodimer adopts an open conformation in our crystals, dimerizing via only one of the two expected interfaces, the subunit cores themselves resemble other SMC hinge domains already described (29,36,37). Interestingly, the SMC2 hinge is more similar to the prokaryotic SMC hinge (29) than the SMC4 hinge. The structural features of the SMC4 hinge that are different from its bacterial counterpart might be involved in specific functions of the condensin complex which the prokaryotic SMC complex does not have. Since these structural features are exposed on the outer surface of the SMC4 hinge, they could constitute a binding interface for an interaction partner like Cti1/C1D, a protein that was found to interact with the SMC4 hinge domain in fission yeast (16) and is implicated in DNA repair functions (58,59). Further research is clearly necessary to find out whether condensin also interacts with C1D in higher eukaryotes, and if so, whether it does this via the SMC4 hinge domain.

The open conformation that we observe in our crystals might be caused by the SMC2–SMC4 hinge domain construct being too short for the second dimerization interface to be stable, but it is also possible that it represents a functional intermediate during assembly of SMC complexes or their action on DNA. The SMC2–SMC4

hinge heterodimer is stable although one dimer interface is disrupted, indicating that one intact interface suffices for dimerization. This observation is in close agreement with mutational studies of the bovine cohesin hinge domain (30). The intact interface between the SMC2 and SMC4 subunit in our structure also offers an explanation as to how dimerization specificity of SMC proteins is created. Comparing the interacting residues with the corresponding residues in SMC1 α and SMC3, we found that some of these residues would either clash with, or not be able to interact with the interface residues of the 'wrong' partners.

The interaction between the two subunits is strong enough to withstand some structural rearrangements, as the interface remains intact despite the hinge being bent open along the interface axis, leading to a wider angle between subunits than in the closed conformation. Our data therefore provide additional evidence for the structural flexibility of the hinge domain, a quality that is probably very important for the dynamic interactions of SMC proteins with DNA (32,60,61). The open conformation we observe would at first glance seem to suggest that the hinge domain could indeed open up to allow DNA to enter into the intra-coiled-coil space, as has been proposed (60). While we do not want to rule out this possibility, the space between the SMC2 and SMC4 subunits in our crystal structure is not big enough to accommodate a DNA double helix, and the charge distribution on the inner surface of the hinge domain would rather repulse than attract DNA (Figure 6A). In fact, the observed charge distribution with only one strongly basic patch argues for a preference for ssDNA over dsDNA.

It has been demonstrated that the transition into the coiled-coil region is necessary for DNA binding by the cohesin hinge, but not for its dimerization (30). Similar results were obtained in a previous study of the BsSMC protein (31), and we found this to be true for the mouse condensin hinge domain as well. In our experiments, the construct without coiled-coil regions bound to DNA only very weakly and non-specifically, whereas the construct carrying a short stretch of coiled-coil bound ssDNA strongly and specifically. Our structural data show that in the construct without coiled-coil regions only one dimer interface is intact, while the longer construct has both expected dimer interfaces. Taken together, these results suggest that the transition into the coiled-coil region does not directly participate in DNA binding, but rather confers structural stability to the hinge domain, especially to the basic patch at the dimer interface which is essential for DNA binding.

The effects of our lysine-to-glutamate mutants of the condensin hinge domain in DNA-binding assays imply that ssDNA wraps around the outer surface of the hinge domain, and all positively charged residues contribute to binding. In spite of prokaryotic SMC proteins also showing a preference for ssDNA over dsDNA, as has been observed previously with the *B. subtilis* SMC (BsSMC) hinge domain (31–33,35), their DNA binding surface is likely to be different. While the outer surface of the condensin hinge domain is neutral-to-positively charged (Figure 6A), the TmaSMC hinge has a neutral-to-negatively charged outer surface, and only its

inner surface is positively charged with the basic patch at the interface also being less pronounced (29). The DNA binding activity of the TmaSMC hinge has never been studied, but due to the strong sequence conservation it is probably quite similar to that of the BsSMC hinge domain, or conversely, the surface charge distributions of both hinge domains are probably quite similar. In studies of the BsSMC protein (32), the authors found a complete disruption of dsDNA binding when the conserved lysine residue K⁵⁶⁵ (corresponding to mSMC2-K⁵⁶⁶/mSMC4-K⁶⁵⁷) was mutated to glutamate, whereas ssDNA binding seemed to be only modestly affected. Only mutation of three consecutive lysine residues (K⁶⁶⁶–K⁶⁶⁸) to glutamate, that are part of the same basic patch at the dimer interface as K⁵⁶⁵, resulted in a complete loss of dsDNA as well as ssDNA binding (32). Our own studies suggest that prokaryotic SMC hinge domains bind DNA with lower affinity than the condensin hinge domain, whilst always having a preference for ssDNA (unpublished data). In prokaryotic SMC proteins, the DNA is therefore probably bound only by the basic patch at the hinge domain dimer interface. Interestingly, studies of the BsSMC protein also suggest that the prokaryotic SMC hinge domain interacts with dsDNA and ssDNA in mechanistically distinct manners (32,33), as our results show the eukaryotic condensin hinge domain does.

What could be the function of the ssDNA binding activity of the condensin hinge domain? We propose that this activity might support the SSB repair function of the condensin complex. In higher eukaryotes, PARP1 recognizes single-strand breaks and facilitates base-excision repair (BER) (26). There are two BER pathways, short- and long-patch BER (26). Short-patch BER repairs single-nucleotide gaps, employing DNA polymerase β and DNA ligase III α . Long-patch BER on the other hand requires the action of FEN1, DNA polymerase δ/ϵ (or β) and DNA ligase I to repair gaps of up to 12 nucleotides length, and is additionally stimulated by PARP1 and PCNA (26). In addition to its interaction with PARP1, upon SSB damage induction condensin was found to interact with the BER scaffold protein XRCC1 as well as FEN1 and DNA polymerase δ/ϵ (25), suggesting it is involved in long-patch BER. The ssDNA binding activity of the condensin hinge domain might tether it to the damage site and might help to organize the DNA structure for repair. This function might also be important during normal DNA replication which transiently produces ssDNA stretches, as suggested by the replication checkpoint defect of condensin mutants (14), and the accumulation of condensin at stalled replication forks (28). Lower eukaryotes like yeast do not possess PARP1, therefore condensin must have a slightly different function in DNA repair in these organisms (14,16). However, it is likely that condensin participates in SSB repair in lower eukaryotes as well, and possibly even in prokaryotes, since prokaryotic SMC hinge domains also preferentially bind ssDNA (31–33). It is conceivable that ssDNA binding has been enhanced during the evolution from prokaryotic SMC proteins to condensin while genome size increased and DNA repair

pathways consequently became more and more sophisticated.

ACCESSION NUMBER

PDB ID code 3L51.

SUPPLEMENTARY DATA

Supplementary Data are available at NAR Online.

ACKNOWLEDGEMENTS

The authors thank Frank Uhlmann for discussions and collaborative support, Alexandra Schele for general assistance in the laboratory, the staff of beamlines X06SA/Swiss Light Source (SLS) and EMBL/DESY X33 for help and support during data collection, Matthew Bennett for critical reading of the manuscript, and the Hopfner group for valuable discussions. J.J.G. thanks the Boehringer Ingelheim Fonds for financial and personal support.

FUNDING

Deutsche Forschungsgemeinschaft (SFBs 646 and 684 and HO2489/3); German Excellence Initiative (Center for Integrated Protein Science Munich and Munich Center for Advanced Photonics); Boehringer Ingelheim Fonds to J.J.G. Funding for open access charge: Deutsche Forschungsgemeinschaft.

Conflict of interest statement. None declared.

REFERENCES

- Hirano, T. (2006) At the heart of the chromosome: SMC proteins in action. *Nat. Rev. Mol. Cell Biol.*, **7**, 311–322.
- Graumann, P.L. and Knust, T. (2009) Dynamics of the bacterial SMC complex and SMC-like proteins involved in DNA repair. *Chromosome Res.*, **17**, 265–275.
- Nasmyth, K. and Haering, C.H. (2009) Cohesin: its roles and mechanisms. *Annu. Rev. Genet.*, **43**, 525–558.
- Hudson, D.F., Marshall, K.M. and Earnshaw, W.C. (2009) Condensin: architect of mitotic chromosomes. *Chromosome Res.*, **17**, 131–144.
- Vagnarelli, P., Hudson, D.F., Ribeiro, S.A., Trinkle-Mulcahy, L., Spence, J.M., Lai, F., Farr, C.J., Lamond, A.I. and Earnshaw, W.C. (2006) Condensin and Repo-Man-PP1 co-operate in the regulation of chromosome architecture during mitosis. *Nat. Cell Biol.*, **8**, 1133–1142.
- Hudson, D.F., Vagnarelli, P., Gassmann, R. and Earnshaw, W.C. (2003) Condensin is required for nonhistone protein assembly and structural integrity of vertebrate mitotic chromosomes. *Dev. Cell*, **5**, 323–336.
- De Piccoli, G., Torres-Rosell, J. and Aragon, L. (2009) The unnamed complex: what do we know about Smc5-Smc6? *Chromosome Res.*, **17**, 251–263.
- Donze, D., Adams, C.R., Rine, J. and Kamakaka, R.T. (1999) The boundaries of the silenced HMR domain in *Saccharomyces cerevisiae*. *Genes Dev.*, **13**, 698–708.
- Horsfield, J.A., Anagnostou, S.H., Hu, J.K., Cho, K.H., Geisler, R., Lieschke, G., Crosier, K.E. and Crosier, P.S. (2007) Cohesin-dependent regulation of Runx genes. *Development*, **134**, 2639–2649.
- Lara-Pezzi, E., Pezzi, N., Prieto, I., Barthelemy, I., Carreiro, C., Martinez, A., Maldonado-Rodriguez, A., Lopez-Cabrera, M. and Barbero, J.L. (2004) Evidence of a transcriptional co-activator function of cohesin STAG/SA/Scs3. *J. Biol. Chem.*, **279**, 6553–6559.
- Rollins, R.A., Korom, M., Aulner, N., Martens, A. and Dorsett, D. (2004) *Drosophila* nipped-B protein supports sister chromatid cohesion and opposes the stromalin/Scs3 cohesion factor to facilitate long-range activation of the *cut* gene. *Mol. Cell. Biol.*, **24**, 3100–3111.
- Bhalla, N., Biggins, S. and Murray, A.W. (2002) Mutation of YCS4, a budding yeast condensin subunit, affects mitotic and nonmitotic chromosome behavior. *Mol. Biol. Cell*, **13**, 632–645.
- Lupo, R., Breiling, A., Bianchi, M.E. and Orlando, V. (2001) *Drosophila* chromosome condensation proteins Topoisomerase II and Barren colocalize with Polycomb and maintain *Fab-7* PRE silencing. *Mol. Cell*, **7**, 127–136.
- Aono, N., Sutani, T., Tomonaga, T., Mochida, S. and Yanagida, M. (2002) Cnd2 has dual roles in mitotic condensation and interphase. *Nature*, **417**, 197–202.
- Birkenbihl, R.P. and Subramani, S. (1992) Cloning and characterization of *rad21* an essential gene of *Schizosaccharomyces pombe* involved in DNA double-strand-break repair. *Nucleic Acids Res.*, **20**, 6605–6611.
- Chen, E.S., Sutani, T. and Yanagida, M. (2004) Cti1/CID interacts with condensin SMC hinge and supports the DNA repair function of condensin. *Proc. Natl Acad. Sci. USA*, **101**, 8078–8083.
- Kim, J.S., Krasieva, T.B., LaMorte, V., Taylor, A.M. and Yokomori, K. (2002) Specific recruitment of human cohesin to laser-induced DNA damage. *J. Biol. Chem.*, **277**, 45149–45153.
- Kim, S.T., Xu, B. and Kastan, M.B. (2002) Involvement of the cohesin protein, Smc1, in Atm-dependent and independent responses to DNA damage. *Genes Dev.*, **16**, 560–570.
- Schar, P., Fasi, M. and Jessberger, R. (2004) SMC1 coordinates DNA double-strand break repair pathways. *Nucleic Acids Res.*, **32**, 3921–3929.
- Sjogren, C. and Nasmyth, K. (2001) Sister chromatid cohesion is required for postreplicative double-strand break repair in *Saccharomyces cerevisiae*. *Curr. Biol.*, **11**, 991–995.
- Strom, L., Lindroos, H.B., Shirahige, K. and Sjogren, C. (2004) Postreplicative recruitment of cohesin to double-strand breaks is required for DNA repair. *Mol. Cell*, **16**, 1003–1015.
- Unal, E., Arbel-Eden, A., Sattler, U., Shroff, R., Lichten, M., Haber, J.E. and Koshland, D. (2004) DNA damage response pathway uses histone modification to assemble a double-strand break-specific cohesin domain. *Mol. Cell*, **16**, 991–1002.
- Strom, L., Karlsson, C., Lindroos, H.B., Wedahl, S., Katou, Y., Shirahige, K. and Sjogren, C. (2007) Postreplicative formation of cohesion is required for repair and induced by a single DNA break. *Science*, **317**, 242–245.
- Unal, E., Heidinger-Pauli, J.M. and Koshland, D. (2007) DNA double-strand breaks trigger genome-wide sister-chromatid cohesion through Eco1 (Ctf7). *Science*, **317**, 245–248.
- Heale, J.T., Ball, A.R. Jr, Schmiesing, J.A., Kim, J.S., Kong, X., Zhou, S., Hudson, D.F., Earnshaw, W.C. and Yokomori, K. (2006) Condensin I interacts with the PARP-1-XRCC1 complex and functions in DNA single-strand break repair. *Mol. Cell*, **21**, 837–848.
- Caldecott, K.W. (2008) Single-strand break repair and genetic disease. *Nat. Rev. Genet.*, **9**, 619–631.
- Ono, T., Losada, A., Hirano, M., Myers, M.P., Neuwald, A.F. and Hirano, T. (2003) Differential contributions of condensin I and condensin II to mitotic chromosome architecture in vertebrate cells. *Cell*, **115**, 109–121.
- D'Ambrosio, C., Schmidt, C.K., Katou, Y., Kelly, G., Itoh, T., Shirahige, K. and Uhlmann, F. (2008) Identification of cis-acting sites for condensin loading onto budding yeast chromosomes. *Genes Dev.*, **22**, 2215–2227.
- Haering, C.H., Lowe, J., Hochwagen, A. and Nasmyth, K. (2002) Molecular architecture of SMC proteins and the yeast cohesin complex. *Mol. Cell*, **9**, 773–788.
- Chiu, A., Revenkova, E. and Jessberger, R. (2004) DNA interaction and dimerization of eukaryotic SMC hinge domains. *J. Biol. Chem.*, **279**, 26233–26242.

31. Hirano, M. and Hirano, T. (2002) Hinge-mediated dimerization of SMC protein is essential for its dynamic interaction with DNA. *EMBO J.*, **21**, 5733–5744.
32. Hirano, M. and Hirano, T. (2006) Opening closed arms: long-distance activation of SMC ATPase by hinge-DNA interactions. *Mol. Cell*, **21**, 175–186.
33. Hirano, M. and Hirano, T. (2004) Positive and negative regulation of SMC-DNA interactions by ATP and accessory proteins. *EMBO J.*, **23**, 2664–2673.
34. Hirano, M., Anderson, D.E., Erickson, H.P. and Hirano, T. (2001) Bimodal activation of SMC ATPase by intra- and inter-molecular interactions. *EMBO J.*, **20**, 3238–3250.
35. Hirano, M. and Hirano, T. (1998) ATP-dependent aggregation of single-stranded DNA by a bacterial SMC homodimer. *EMBO J.*, **17**, 7139–7148.
36. Ku, B., Lim, J.H., Shin, H.C., Shin, S.Y. and Oh, B.H. (2009) Crystal structure of the MukB hinge domain with coiled-coil stretches and its functional implications. *Proteins*, 10.1002/prot.22664.
37. Li, Y., Schoeffler, A.J., Berger, J.M. and Oakley, M.G. (2010) The crystal structure of the hinge domain of the *Escherichia coli* structural maintenance of chromosomes protein MukB. *J. Mol. Biol.*, **395**, 11–19.
38. Schmidt, T.G., Koepke, J., Frank, R. and Skerra, A. (1996) Molecular interaction between the Strep-tag affinity peptide and its cognate target, streptavidin. *J. Mol. Biol.*, **255**, 753–766.
39. LeMaster, D.M. and Richards, F.M. (1985) 1H-15N heteronuclear NMR studies of *Escherichia coli* thioredoxin in samples isotopically labeled by residue type. *Biochemistry*, **24**, 7263–7268.
40. Gasteiger, E., Hoogland, C., Gattiker, A., Duvaud, S., Wilkins, M.R., Appel, R.D. and Bairoch, A. (2005) Protein identification and analysis tools on the ExPASy server. In Walker, J.M. (ed.), *The Proteomics Protocols Handbook*. Humana Press, pp. 571–607.
41. Laemmli, U.K. (1970) Cleavage of structural proteins during the assembly of the head of bacteriophage T4. *Nature*, **227**, 680–685.
42. Konarev, P.V., Petoukhov, M.V., Volkov, V.V. and Svergun, D.I. (2006) ATSAS 2.1, a program package for small-angle scattering data analysis. *J. Appl. Cryst.*, **39**, 277–286.
43. Wriggers, W. and Chacon, P. (2001) Using Situs for the registration of protein structures with low-resolution bead models from X-ray solution scattering. *J. Appl. Cryst.*, **34**, 773–776.
44. Kabsch, W. (1993) Automatic processing of rotation diffraction data from crystals of initially unknown symmetry and cell constants. *J. Appl. Cryst.*, **26**, 795–800.
45. Vonrhein, C., Blanc, E., Roversi, P. and Bricogne, G. (2007) Automated structure solution with autoSHARP. *Methods Mol. Biol.*, **364**, 215–230.
46. Collaborative Computational Project, N. (1994) The CCP4 suite: programs for protein crystallography. *Acta Cryst. D*, **50**, 760–763.
47. Murshudov, G.N., Vagin, A.A. and Dodson, E.J. (1997) Refinement of macromolecular structures by the maximum-likelihood method. *Acta Cryst. D*, **53**, 240–255.
48. Perrakis, A., Morris, R. and Lamzin, V.S. (1999) Automated protein model building combined with iterative structure refinement. *Nat. Struct. Biol.*, **6**, 458–463.
49. Emsley, P. and Cowtan, K. (2004) Coot: model-building tools for molecular graphics. *Acta Cryst. D*, **60**, 2126–2132.
50. Brunger, A.T., Adams, P.D., Clore, G.M., DeLano, W.L., Gros, P., Grosse-Kunstleve, R.W., Jiang, J.S., Kuszewski, J., Nilges, M., Pannu, N.S. et al. (1998) Crystallography & NMR system: a new software suite for macromolecular structure determination. *Acta Cryst. D*, **54**, 905–921.
51. Afonine, P.V., Grosse-Kunstleve, R.W. and Adams, P.D. (2005) The Phenix refinement framework. *CCP4 Newsl.*, **42**, contribution 8.
52. Davis, I.W., Leaver-Fay, A., Chen, V.B., Block, J.N., Kapral, G.J., Wang, X., Murray, L.W., Arendall, W.B. 3rd, Snoeyink, J., Richardson, J.S. et al. (2007) MolProbity: all-atom contacts and structure validation for proteins and nucleic acids. *Nucleic Acids Res.*, **35**, W375–W383.
53. Laskowski, R.A., MacArthur, M.W., Moss, D.S. and Thornton, J.M. (1993) Procheck – a program to check the stereochemical quality of protein structures. *J. Appl. Cryst.*, **26**, 283–291.
54. Baker, N.A., Sept, D., Joseph, S., Holst, M.J. and McCammon, J.A. (2001) Electrostatics of nanosystems: application to microtubules and the ribosome. *Proc. Natl Acad. Sci. USA*, **98**, 10037–10041.
55. Kibbe, W.A. (2007) OligoCalc: an online oligonucleotide properties calculator. *Nucleic Acids Res.*, **35**, W43–W46.
56. Cobbe, N. and Heck, M.M. (2004) The evolution of SMC proteins: phylogenetic analysis and structural implications. *Mol. Biol. Evol.*, **21**, 332–347.
57. Overman, L.B., Bujalowski, W. and Lohman, T.M. (1988) Equilibrium binding of *Escherichia coli* single-strand binding protein to single-stranded nucleic acids in the (SSB)65 binding mode. Cation and anion effects and polynucleotide specificity. *Biochemistry*, **27**, 456–471.
58. Erdemir, T., Bilican, B., Cagatay, T., Goding, C.R. and Yavuzer, U. (2002) *Saccharomyces cerevisiae* C1D is implicated in both non-homologous DNA end joining and homologous recombination. *Mol. Microbiol.*, **46**, 947–957.
59. Yavuzer, U., Smith, G.C., Bliss, T., Werner, D. and Jackson, S.P. (1998) DNA end-independent activation of DNA-PK mediated via association with the DNA-binding protein C1D. *Genes Dev.*, **12**, 2188–2199.
60. Gruber, S., Arumugam, P., Katou, Y., Kuglitsch, D., Helmhart, W., Shirahige, K. and Nasmyth, K. (2006) Evidence that loading of cohesin onto chromosomes involves opening of its SMC hinge. *Cell*, **127**, 523–537.
61. Onn, I., Aono, N., Hirano, M. and Hirano, T. (2007) Reconstitution and subunit geometry of human condensin complexes. *EMBO J.*, **26**, 1024–1034.
62. Corpet, F. (1988) Multiple sequence alignment with hierarchical clustering. *Nucleic Acids Res.*, **16**, 10881–10890.